

Microwave Generation by an Intense Relativistic Electron Beam

メタデータ	言語: eng 出版者: 公開日: 2017-10-03 キーワード (Ja): キーワード (En): 作成者: 川崎, 温, 鎌田, 啓一, 増崎, 克 メールアドレス: 所属:
URL	https://doi.org/10.24517/00011224

This work is licensed under a Creative Commons Attribution-NonCommercial-ShareAlike 3.0 International License.



Microwave Generation by an Intense Relativistic Electron Beam

Ichiro AOKI*, Sunao KAWASAKI, Keichi KAMADA and Masaru MASUZAKI

Department of Physics, Kanazawa University
(Kanazawa 920, Japan)

Abstract Comparatively studied was the mechanism of high power electromagnetic wave radiation in various resonating structures. The typical working parameters of the beam are the peak currents of 4 kA and the particle energies of 200keV, and it has an annular density distribution of 1.9cm radius and ~2mm width in 3kG linear guide field. The linear theories of the electron beam instabilities in the surrounding pumping fields are developed and compared with the frequency spectra of the resulted radiation, which was analysed mainly in X-band up to 20 GHz using a long dispersive waveguide line technique. At the observed power level (0.1MW maximum power), the theory seems to be consistent with the experimental results qualitatively.

I. INTRODUCTION

Intense relativistic electron beam (REB) accelerators have many potential applications to high power pulse studies; high-power microwave radiations, collective ion acceleration, etc. In recent years, generation of microwaves is taken much interest. Because of high power and fast velocity of REB, high-power bursts of microwave radiations by REB can be expected. Typical arrangements of microwave generation by REB were i) slow wave structures like a disk-loaded waveguide¹⁻²⁾ or an acrylic cylindrical waveguide³⁾, ii) beam cyclotron structures like a rippled magnetic field waveguide⁴⁻⁹⁾. The radiation occurs at a frequency such that the phase velocities of the cyclotron and/or the space-charge wave on the beam plasma and a low-order TE or TM mode in the waveguide are equal.

In this paper, high-power microwave radiation in the X-band is studied, where a pulsed relativistic electron beam propagated through four types of cylindrically symmetric waveguides: a simple smooth metallic waveguide (drift tube), a rippled magnetic field waveguide, a dielectric loaded waveguide and a disk-loaded waveguide. The experimental apparatus is described in Sec. II. The mechanism of microwave

* Present address: Tigold Corporation, Sanbu-Machi, Chiba, 289-12

radiation is considered in Sec. III and experimental results are given in Sec. IV. Section V is devoted to discussion of the results. The present work is summarized in Sec. VI.

II. EXPERIMENTAL APPARATUS

The whole experimental configuration is shown in Fig. 1. Figure 2 shows in the vicinity of the diode and the drifttube.

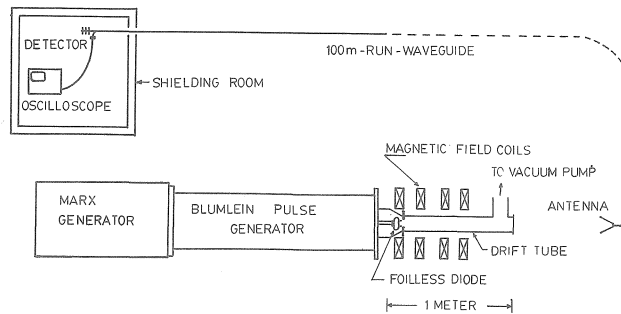


Fig. 1 Experimental configuration of microwave generation. The dispersive line is a 100-m length of X-band waveguide.

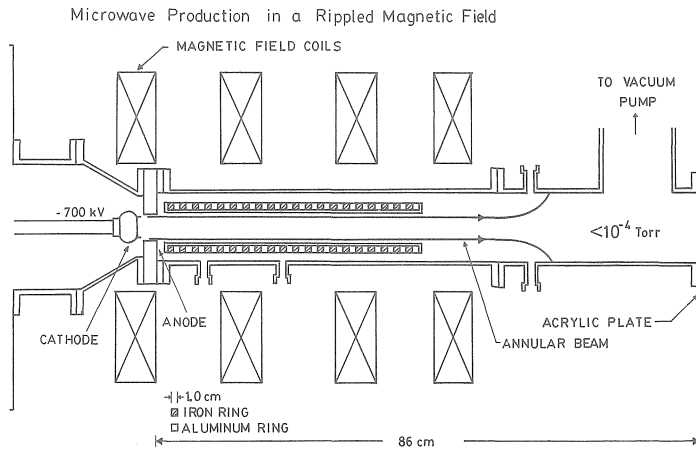


Fig. 2 Experimental apparatus: diode, magnetic field coils, and rippled magnetic field structure inserted in the drift tube. 1 and 2 represent the positions of magnetic pick-up loops.

II-i) BEAM SOURCE

REB is generated by an electron-accelerator system called the Model 105 A Pulserad produced by the Physics International Company. The 105 A Pulserad consists of three main parts; 1) the energy source, a Marx generator (0.5MV, 1.25kJ), 2) the pulse forming line, a coaxial Blumlein line (40ohms), 3) the field emission diode. The structure

and operation of the Model 105 A Pulserad are discussed in detail in Reference 10. The diode used in the experiment is made of stainless-steel and is a foilless type with a circular knife-edge cathode (see Fig. 2). The radius of the cathode edge is 1.9cm. This REB generator has the following characteristics; the peak current I_D is typically 10 kA, the peak voltage V_D is typically 0.7MV, the pulse-width (FWHM) is 10 nsec for approximately 25 nsec total duration. Typical wave form is shown in Fig. 3.

II-ii) PROPAGATING BEAM

The annular electron beam propagates through the cylindrical drift tube with an external magnetic field up to 3 kG. Without the magnetic field, comparatively small current was detected by the magnetic probe installed near the end of the tube (Fig. 4). The beam propagation was confirmed in measurements with both magnetic probes and a damage pattern on a acrylic plate of 2mm thickness. The probe is one-turn magnetic pick up loop made of microcoaxial cable (UT-85C). The beam current injected into the drift tube was ~ 4 kA, and the damage patterns shown in Fig. 5 indicate the diameter of ~ 3.7 cm and the beam thickness of ~ 2 mm. The magnetic field strength is shown in Fig. 6 as a function of axial distance. We treated this magnetic field as a linear guide field.

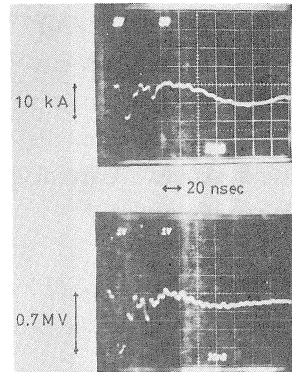


Fig. 3 Current and voltage traces of the electron beam accelerator.

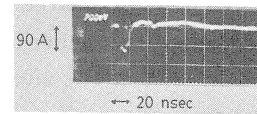


Fig. 4 Current trace when the guide field was not applied.

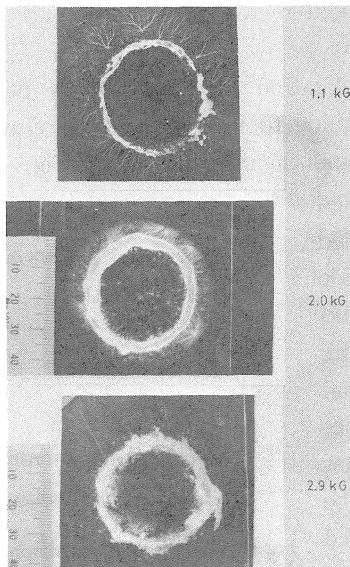


Fig. 5 Damage pattern on an acrylic plate caused by the annular beam. Each plate was located 3-cm down stream.

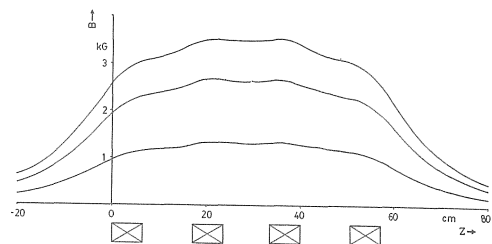


Fig. 6 Approximate dc magnetic field strength.

II-iii) BEAM VELOCITY

The beam velocity was determined by the time-of-flight method. Two magnetic probes were mounted at the positions 1 and 2 (41.5-cm apart from each other) in Fig. 2. The signals from the probes were observed by the Tektronix 7844 Dual-Beam Oscilloscopes. Careful cable setting was done to measure the time difference of very short pulses.

II-iv) BEAM DENSITY

The value of the beam density n_e are derived from

$$I_b = 2\pi e \int_{R_0}^{R_p} r dr n_e(r) v(r) \quad , \quad (1)$$

where e is the charge of an electron, r is the radial distance from the cylindrical axis, $n_e(r)$ is the beam density, $v(r)$ is the beam velocity, R_p is the outer radius and R_0 is the inner radius of the annular beam. The radii R_p and R_0 were determined by the damage pattern size (see Fig. 5) It is assumed that the axial velocity and density profiles are independent of distance r from the axis of symmetry of the electron column, that is,

$$v(r) = v = \text{const.} \quad , \quad n_e(r) = n_e = \text{const.}$$

From this assumption the beam density n_e (and the electron plasma frequency ω_{pe}) is calculated from the measurement values I_b and v .

II-v) RESONATORS FOR *rf*-WAVE RADIATION

The beam was injected into evacuated cylindrical metallic chamber with 10.8cm diameter. The base pressure in the chamber was below 1.0×10^{-4} Torr. This is sufficiently low vacuum that space-charge neutralization of the electron beam is negligible in the chamber¹¹⁾. Three types of waveguide to interact with a relativistic annular electron layer were inserted into this smooth metallic tube (Fig. 2); 1) cylindrical waveguide which has a structure of rippled magnetic field (Fig. 7-1), 2) cylindrical dielectric loaded waveguide (Fig. 7-2), 3) apertured disk-loaded waveguide (Fig. 7-3). Each waveguide had the length of 40cm and the outer diameter of 8cm (the inner diameter is 5cm) and was inserted to be immersed in the external magnetic field. The periodic structures of waveguides 1) and 3) were repeated twenty and forty times respectively. Without these resonators, the drift tube acted as a simple cylindrical waveguide and interacted with a beam layer. Thus four types of waveguide were utilized.

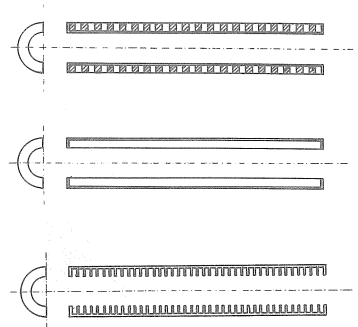


Fig. 7 Waveguides as resonators. 1) rippled magnetic field waveguide, 2) dielectric loaded waveguide, 3) diskloaded waveguide.

II-vi) RF-WAVE MEASUREMENT

To measure the spectral distribution of the emitted rf waves, the apparatus described below was utilized. A rectangular receiving antenna ($11.6 \times 14.3 \text{ cm}^2$) which was 15cm apart from the acrylic vacuum window (5mm thick, the absorption of rf wave by the window is negligible) was used. Because of intense ($\sim 0.1 \text{ MW}$) and short ($\sim 10 \text{ nsec}$) pulse signal, a long waveguide (100m) was used to disperse and attenuate the rf wave¹²⁾ (Figure 8 shows the signals and without long waveguide.).

The microwave signals were monitored by a X-band crystal detector (NEC, IN23C) after propagation in the long waveguide. And the signals were observed by the oscilloscope. Each frequency has a different propagation velocity in a waveguide so that a spectral distribution is transformed into a distribution in propagation time. Thus frequency can determine by observing the transit time t ;

$$f = \frac{f_c}{\sqrt{1-(l/tc)^2}} \quad (2)$$

where f_c is the cut-off frequency of the guide, l is the length of the long guide and c is the light velocity.

To determine the emitted microwave mode, (TE_{01} or TM_{01} mode [symmetrical modes] is the most probable in our experiment.) a twisted waveguide was used. This guide was mounted between the receiving horn and the edge of the dispersive line. If the emitted microwave had an unsymmetrical mode (TE_{11} , TM_{11} , etc.), different frequencies would be observed by use of this twisted guide. The observed transit time, however, did not change whether or not the twisted guide was used in the whole experiment. These observations indicated that the most probable mode was a symmetrical one.

Total X-band power P obtained from sum of the power of the individual peak $p_i(\omega)$ (the attenuation factors of waveguide for each frequency were taken into account);

$$P = \sum_i p_i(\omega) \quad (3)$$

III. MECHANISM OF RF-WAVE RADIATION

A relativistic electron beam propagates through a waveguide (drift tube) along an applied axial magnetic field B . As the waveguide is in vacuum ($< 10^{-4}$ Torr), two-stream instabilities are not present. The waveguide modes interact unstably with beam waves on the nonneutral relativistic electron beam. Two types of interaction are

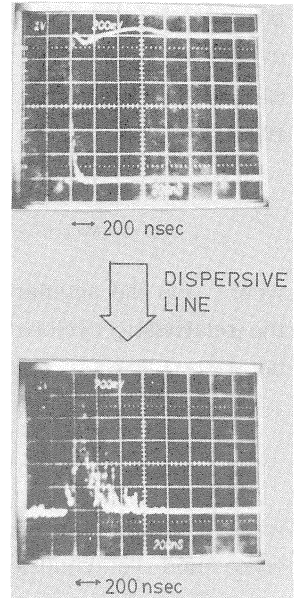


Fig.8 Comparison between a dispersed microwave signal and a nondispersed one. The effect of the dispersive line appears in the lower picture.

possible in the cylindrical waveguide. These are the interactions between the cyclotron¹³⁾ or space-charge¹⁴⁾ wave and the waveguide modes. The cyclotron and space-charge waves for sufficiently small density have following dispersion relations, respectively ;

$$\omega = kv_b + \Omega, \quad (4)$$

$$\omega = kv_b + \omega_{pe}^*, \quad (5)$$

where ω is the angular frequency, k is the wave number, v_b is the beam velocity, Ω is the relativistic cyclotron frequency and ω_{pe}^* is the reduced plasma frequency. In this notation Ω and ω_{pe}^* represent using the relativistic factor γ ($\gamma = \{1 - (v_b/c)^2\}^{-1/2}$),

$$\begin{aligned} \Omega &= \omega_{ce} / \gamma, \\ \omega_{pe}^* &= \omega_{pe} / \gamma^{3/2}, \end{aligned}$$

where ω_{ce} is the beam cyclotron frequency and ω_{pe} the beam plasma frequency. On the other hand the cylindrical waveguide modes are expressed as

$$\omega^2 = k^2 c^2 + \omega_{c0}^2, \quad (6)$$

where ω_{c0} is the cut-off frequency of the waveguide.

The instability owing to cyclotron wave was investigated theoretically by Ott and Manheimer¹³⁾. They assumed that the instabilities that the waveguide mode could interact unstably with the beam by resonating with the cyclotron wave were driven by sources of free energy inherent in the electron beam distribution function. Such a source has the anisotropy of the particle distribution arising from the exceeding energy spread. They calculated the dispersion relation for a planar sheet beam in a parallel plate waveguide because of analytical tractability. Hence their results are not immediately applicable to our cylindrical geometry.

From the conventional analysis¹⁴⁾ of the coupling of an electron beam to a slow wave structure, cumulative interaction between the two waves occurs when the phase velocity of the space-charge wave is nearly equal to the phase velocity of a slow-wave structure mode. As electromagnetic waves with TM modes propagate in the slow wave structure (a disk-loaded waveguide, a dielectric loaded waveguide), rf-waves with TM modes would be emitted.

For the interaction between the cyclotron waves and the waveguide modes, the expected frequency would be found from the simultaneous solutions of Eqs. 4 and 6 ;

$$\omega = \frac{\Omega}{1-\beta^2} \left[1 \pm \beta \left\{ 1 - (1-\beta^2) \frac{\omega_{c0}^2}{\Omega^2} \right\}^{1/2} \right], \quad (7)$$

and for the space-charge wave interaction, from Eqs. 5 and 6 ;

$$\omega = \frac{\omega_{pe}^*}{1-\beta^2} \left[1 \pm \beta \left\{ 1 - (1-\beta^2) \frac{\omega_{c0}^2}{\Omega^2} \right\}^{1/2} \right], \quad (8)$$

where $\beta = v_b/c$. In these expression the minus and plus signs correspond to backward and forward waves, respectively. It is possible to couple to either wave. The possible resonance points between the beam waves and the waveguide dispersion curve are shown schematically in Fig. 9. Dispersion curves for various cylindrical waveguides are given by modifying Eq. 6.

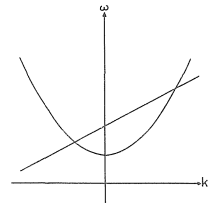


Fig. 9 Intersection of the waveguide mode with the cyclotron or the space-charge wave.

IV. EXPERIMENTAL RESULTS

As described in Sec. II, we carried out an experiment by use of four types of waveguide resonators to interact with a relativistic annular electron beam. The experimental work was carried out at a gas pressure of $<10^{-4}$ Torr.

50-cm long smooth metallic waveguide (drift tube) was immersed in an approximate dc magnetic field (see Fig. 6). The whole drift tube is 86cm long. Figure 10 shows the

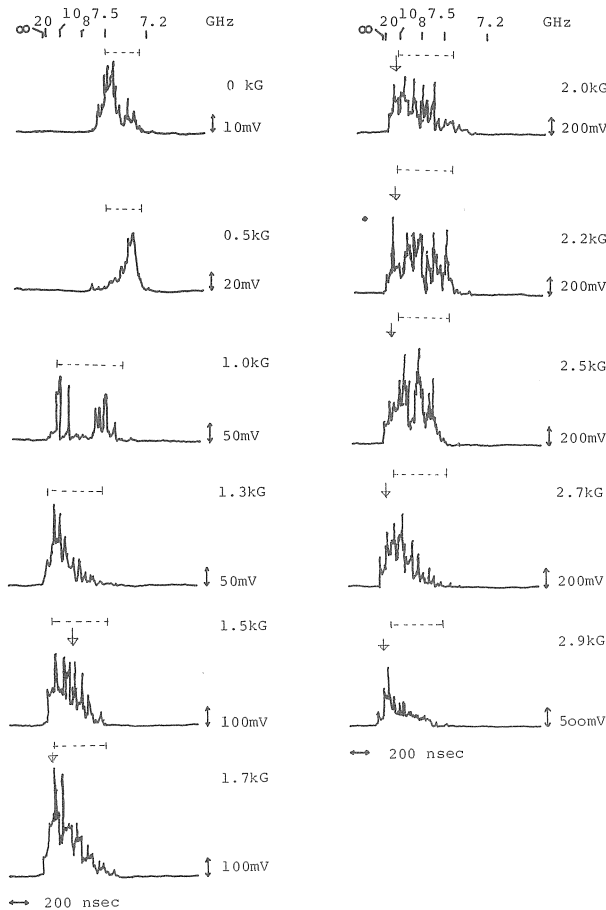


Fig.10 Microwave signals from the smooth metallic waveguide as a parameter of the guide field.

typical traces of rf signal where the B strength is the parameter. It is apparently shown that the amplitudes and frequencies increase gradually as the guide field increases. By use of Eq. 2 the horizontal axis interprets to the frequencies. The frequency scale is shown at the upper end of the figure. As frequency go up, however, plotting error becomes greater as shown in Fig. 11.

Other waveguides as resonators were inserted in the drift tube at a distance of 2cm away from the anode. (dielectric loaded waveguide is 1-cm away) Figure 2 shows the schematic configuration of the rippled field waveguide. The electron beam passed through a resonator was monitored by the magnetic probe at the position 2 in Fig. 2. The traced signal from the rippled magnetic field waveguide is shown in Fig. 12. At the guide field range of $0 \rightarrow \sim 2.1$ kG the signals were small. In the case of the dielectric loaded waveguide, the frequencies are nearly constant in spite of increasing the strength of B as shown in Fig. 13. Figure 14 shows the microwave signals from the disk-loaded waveguide. In this case the frequency dependency of the magnetic field is

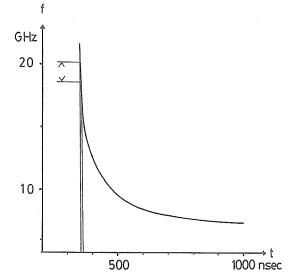


Fig.11 Frequency of rf-wave vs. propagation time after running 100-m-long waveguide.

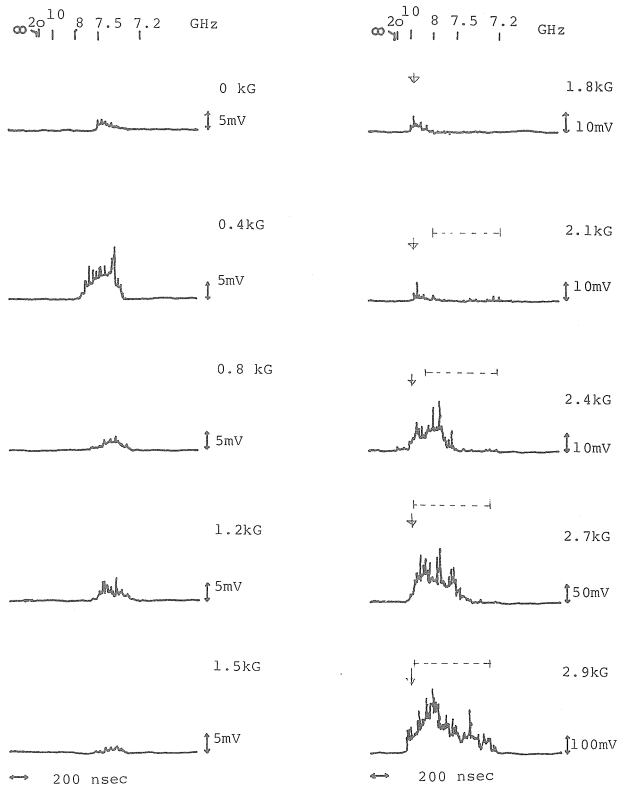


Fig.12 Microwave signals from the rippled field waveguide as a parameter of the guide field.

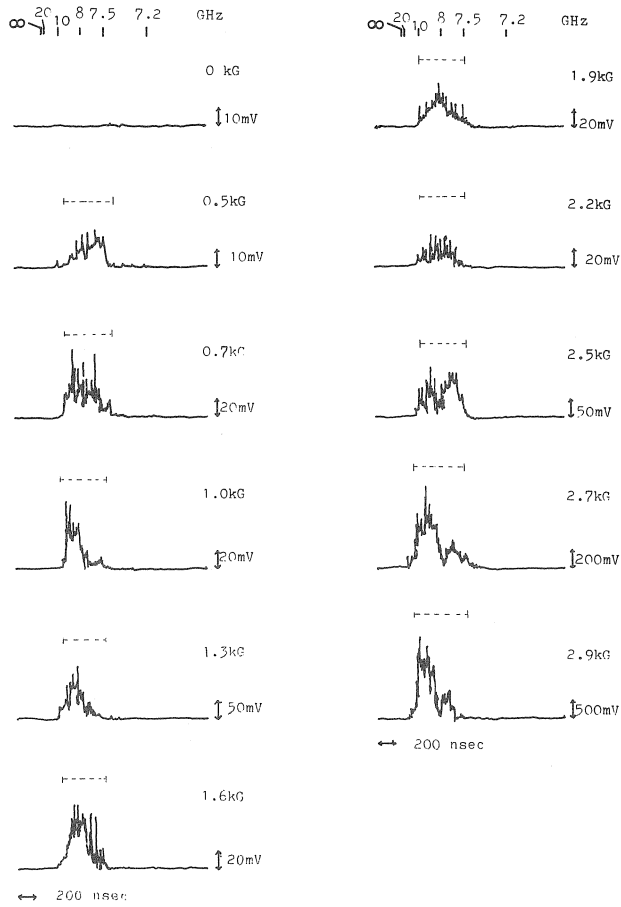


Fig.13 Microwave signals from the dielectric loaded waveguide as a parameter of the guide field.

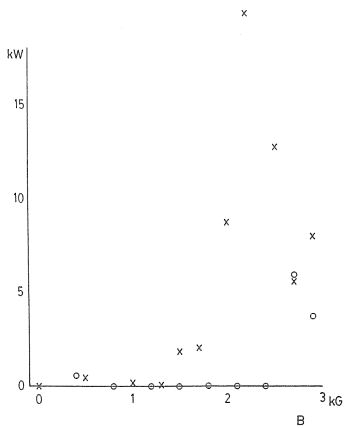


Fig.15 Microwave power as a function of the guide field. Microwave radiation x: from the smooth metallic waveguide, o: from the rippled magnetic field waveguide.

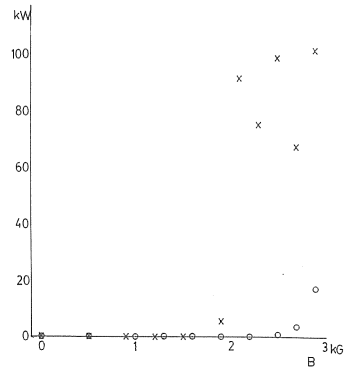


Fig.16 Microwave power as a function of the guide field. Microwave radiation x: from the disk-loaded waveguide, o: from the dielectric loaded waveguide.

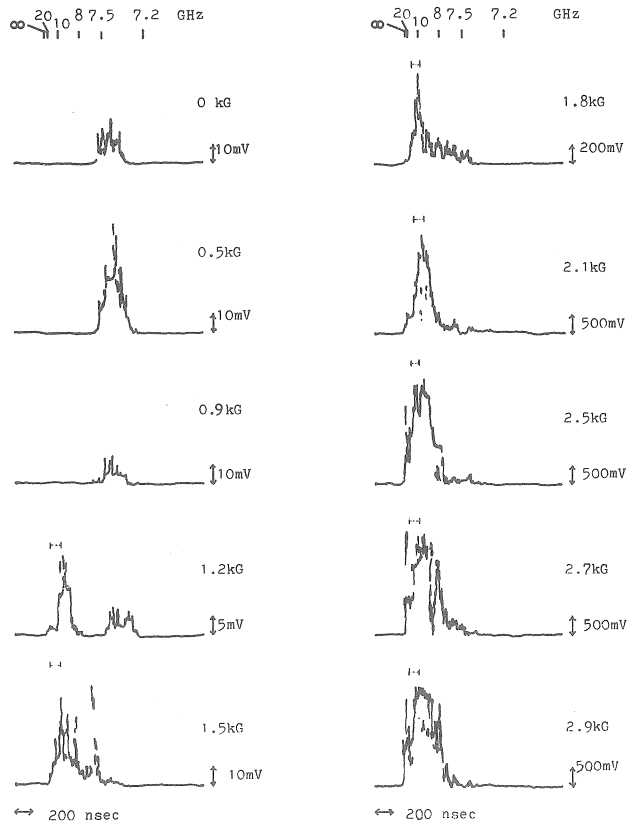


Fig.14 Microwave signals from the disk-loaded waveguide as a parameter of the guide field.

approximately constant. The high intensity signals were observed at the higher magnetic field (>1.8 kG).

Figures 15 and 16 depict the radiated power as a function of B for each ease. High-power microwave generation with the disk-loaded waveguide was obtained (~ 0.1 MW maximum power) and this is shown in Fig. 16. As shown there the power increases as the strength of B increases.

V. DISCUSSION

We now discuss the results of our experiment and compare them with the simple models for each resonating structure.

V-i) SMOOTH METALLIC WAVEGUIDE (DRIFT TUBE)

Two type of frequency mode appear in the experimental result (Fig. 10). One is the mode which scarcely depends upon the guided magnetic field. The frequencies of this mode are near 7.5 GHz in the figure. Another depends upon the strength of magnetic

field, i.e., higher frequencies appear as the strength of magnetic field increases.

To investigate these frequency modes, let us consider the interaction between cylindrical waveguide modes and beam waves as described in Sec. III. Dispersion curves of this system are shown in Fig. 17. The cut-off frequency of the waveguide mode is $\omega_{c0}/2\pi=3.39$ GHz for TE₀₁ mode (: the bottom point of the hyperbola curve in Fig. 17). Straight solid lines and dashed line imply cyclotron and space-charge wave, respectively. Intersections of the straight lines with the curved line indicate the resonance points.

At first, we treat the space-charge wave interaction. In Fig. 17 we treated as the beam is monoenergetic and has constant density distribution. As a space-charge wave in Eq. 5 does not "directly" connect with the applied magnetic field, the intersection between Eqs. 5 and 6 remains constant, which comes out at ~ 7.5 GHz in Fig. 17. In our experiment, since the beam density depends upon the strength of lower guide field as shown in Fig. 18, so the frequency owing to space-charge wave is not constant. From

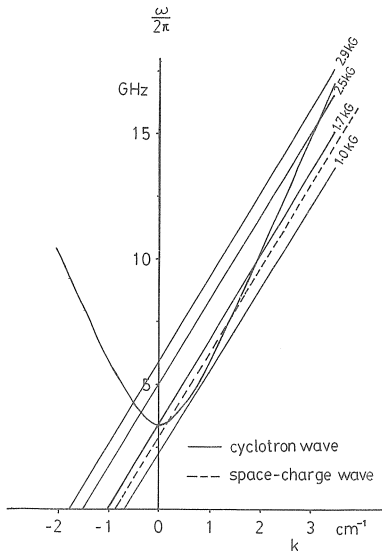


Fig.17 Intersections between beam waves and TE₀₁ waveguide mode. Curved line: waveguide mode, straight solid lines: cyclotron waves, straight dashed line: space-charge wave.

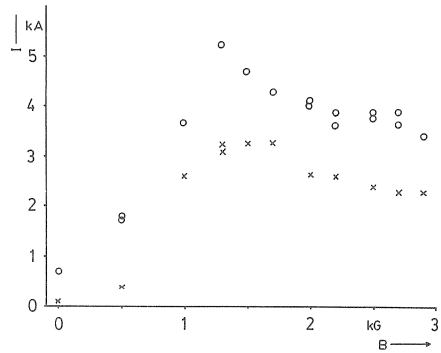


Fig.18 Propagating beam currents monitored by the magnetic probes in the drift tube. These currents were picked up at the position 1 (o marked) and 2 (x marked) in Fig. 2.

the value of the beam plasma frequency calculated by Eq. 1 the points of interaction between space-charge wave and waveguide mode were roughly estimated in Fig. 10 (Dashed line region). The cut-off frequency of the dispersive line is 7.0 GHz, so that frequencies below this value do not observed.

Second, cyclotron wave interactions are treated. Strong dependency for the guide field comes out above 1 kG in Fig. 10. As the intersection will exist if the guide field is beyond 1 kG in Fig. 17, cyclotron wave resonances would be expected for this system. Arrows in Fig. 10 show the calculated cyclotron resonance points for the each guide field strength. These points show fairly agreement with the experimental data.

V-ii) RIPPLED MAGNETIC FIELD WAVEGUIDE

Waves propagating through a periodic structure were affected by the magnetic ripple (Fig. 7-1). Cyclotron waves are modified by the presence of the magnetic ripple,

$$\omega = (k + k_r) v_b + \Omega \quad (9)$$

where k_r is the wave number of the rippled section. The ripple wave number for our experiment is $k_r = 3.14 \text{ cm}^{-1}$.

The effect of the guide field appeared in the higher field ($>1.8 \text{ kG}$) in our experiment as shown in Fig. 12. The intersections of beam waves with waveguide modes in Fig. 19 are investigated below. The cut-off frequency of this rippled waveguide becomes $\omega_{c0}/2\pi = 7.32 \text{ GHz}$ for TE_{01} mode. The possible interaction points for the cyclotron waves (Eq. 9, plotted with solid lines in Fig. 19) are depicted in Fig. 12 (arrows) as a function of the guide field. The effect of the ripple, however, should not appear if the guide field is weak, because the rippled field strength ΔB is very small in comparison with the strength of the applied field B ($\Delta B \ll B$). The ripple percent $\Delta B/B$ was measured about 1% at the guide field $B = 1.5 \text{ kG}$. Experimentally the ripple effect was detected in the higher field strength ($>1.8 \text{ kG}$) as shown in Fig. 12.

Space-charge resonance can expect as the guide field increases (i.e., increase of beam density) as described in Sec. V-i. The relation between the guide field and the beam current is shown in Fig. 20. These currents were picked up the magnetic probe at the position 2 in Fig. 2 after passing through each resonator. The currents through the ripple structure were depicted as small triangles in Fig. 20. From this results, estimated resonant points of space-charge waves were shown in Fig. 19 (Dashed lines). The interaction points for higher field should appear, whose region is drawn in Fig. 12

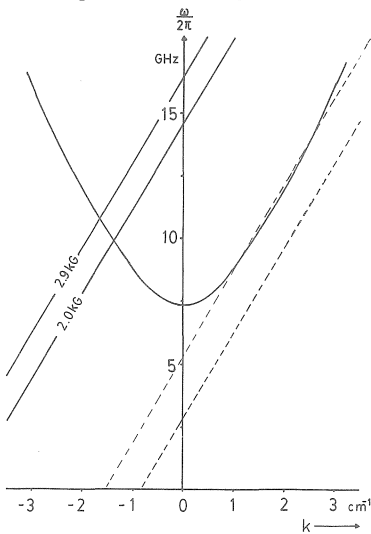


Fig.19 Intersections between beam waves and TE_{01} waveguide mode. Curved line: waveguide mode, straight solid lines: cyclotron waves, straight dashed lines: space-charge waves.

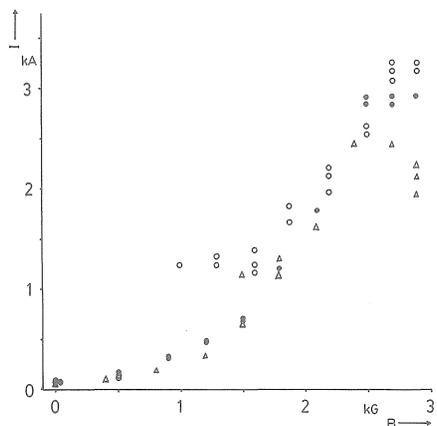


Fig.20 Beam currents monitored by the magnetic probes after passing through each resonator. Currents passed through the rippled magnetic field waveguide (Δ marked), the dielectric loaded waveguide (\circ marked) or the disk-loaded waveguide (\bullet marked).

(Dashed line region). The frequency mode which appears independently of the guide field near 7.5 GHz must be the microwave radiation from the background drift tube.

V-iii) DIELECTRIC LOADED WAVEGUIDE

A hollow dielectric plugged up a stainless tube was used (Fig. 7-2). The inner and outer radii of this dielectric (acryl) are 2.5cm and 3.8cm, respectively. The dispersion curve Eq. 6 of a waveguide is modified by the presence of a dielectric load ;

$$\omega^2 = \omega_{c0}^2 + \eta^2 k^2 c^2 \quad , \quad (10)$$

where ω_{c0} and η are the effective cut-off frequency and the slowing factor, respectively. The effect of a dielectric load is contained in the factor η . The value of these are $\omega_{c0}/2\pi = 3.3$ GHz and $\eta = 0.87$ for the used dielectric loaded waveguide. In the cause of the slowing factor the phase velocity of electromagnetic waves in the guide is smaller than the velocity of light (a slow wave structure). The possible resonance points for this system (the intersection of the space-charge wave with this guide mode) indicated in Fig. 13 (estimated by the beam current [small circles in Fig. 20] and the damage patterns). The effect of the density increase comes out a little in the higher field. All data were explained by the space-charge wave interaction.

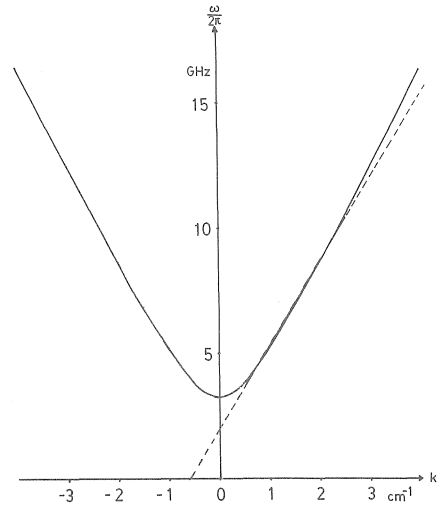


Fig.21 Intersection between space-charge wave (dashed line) and the dielectric loaded waveguide (solid curve).

V-iv) DISK-LOADED WAVEGUIDE

The same treatment was carried out for this system, that is, the intersection between beam waves and the disk-loaded waveguide mode was investigated. With the aid of the parameters indicated in Fig. 23, the dispersion curve for an apertured-disk structure is¹⁵⁻¹⁶⁾

$$\frac{1}{\zeta} \frac{J_1(\frac{\omega}{c}a) N_0(\frac{\omega}{c}b) - N_1(\frac{\omega}{c}a) J_0(\frac{\omega}{c}b)}{J_0(\frac{\omega}{c}a) N_0(\frac{\omega}{c}b) - N_0(\frac{\omega}{c}a) J_0(\frac{\omega}{c}b)} = \frac{\omega}{c} \frac{I_1(\Gamma a)}{\Gamma I_0(\Gamma a)} \quad , \quad (11)$$

where

$$\zeta = (1-d)/l \quad \text{and} \quad \Gamma^2 = k^2 - (\omega/c)^2 \quad .$$

In the above equation, J, N and I are the Bessel functions and ω and k represent the angular frequency and wave number, respectively. The curves obtained from Eq. 11 and the space-charge wave for our system are described in Fig. 22. The intersection

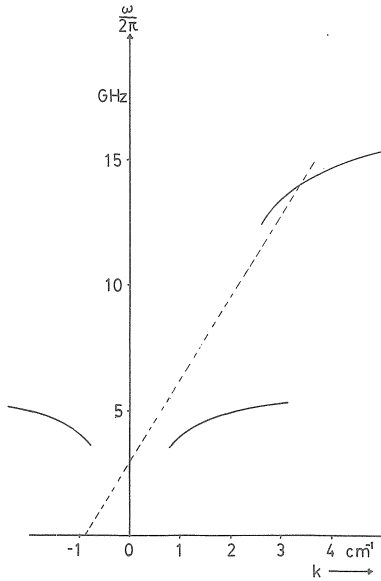


Fig.22 Intersection between space-charge wave (dashed line) and the disk-loaded waveguide (solid curves).

appears near 14 GHz and experimentally the peaks appear around these frequencies (Fig. 14). In Fig. 14 dashed line region means calculated space charge wave resonance points. High-power radiation was obtained from this system. The power was the strongest in the four resonators. We can expect the further strong power radiation by increasing the guide field as shown in Fig. 16.

VI. SUMMARY

It was qualitatively found that microwave generation by REB was the result of interaction between cyclotron or space charge waves and cylindrical waveguide modes. The experimental data showed fair agreement with the calculated values with simple beam models. It was not solved that generated microwaves have a wide spectrum. The necessity of more exact understanding of the nonlinear effects by numerical methods is strongly suggested. This will be our future problem. We showed the possibility of efficient microwave generation by REB with stronger magnetic field. The most efficient generation of microwave radiation was obtained from the disk-loaded waveguide (~ 0.1 MW maximum power). Better efficiency would be expected by stronger magnetic field.

Acknowledgements

The authors thank to Mr. Y. Tamagawa, Mr. S. Ohta, Mr. M. Kihara, Mr. S. Watanbe and Mr. N. Matsuura for their helpful assistance and discussions.

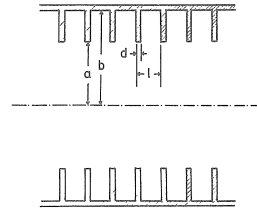


Fig.23 Apertured-disk structure with parameters $a=2.5\text{cm}$, $b=3.8\text{cm}$, $d=0.2\text{cm}$ and $l=M.0\text{cm}$.

References

- 1) J. A. Nation, Appl. Phys. Lett. **17** (1970), 491
- 2) Y. Carmel, J. Ivers, R. E. Kribel and J. Nation, Phys. Rev. Lett. **33** (1974), 1278
- 3) J. E. Walsh, T. C. Marshall and S. P. Schlesinger, Phys. Fluids **20** (1977), 709
- 4) M. Friedman and M. Herndon, Phys. Rev. Lett. **28** (1972), 210
- 5) M. Friedman and M. Herndon, Phys. Rev. Lett. **29** (1972), 55
- 6) M. Friedman and M. Herndon, Phys. Fluids **16** (1973), 1982
- 7) Y. Carmel and J. A. Nation, J. Appl. Phys. **12** (1973), 5268
- 8) V. L. Granatstein, M. Herndon, P. Sprangle, Y. Carmel and J. A. Nation, Plasma Phys. **17** (1975), 23
- 9) W. M. Manheimer and E. Ott, Phys. Fluids **17** (1974), 463
- 10) T. Fujii, Master's Thesis, Kanazawa University (1979) [in Japanese]
- 11) C. L. Olson, Phys. Rev. A, **11** (1975), 288
- 12) J. Nation, Rev. Sci. Instrum. **41** (1970), 1097
- 13) E. Ott and W. M. Manheimer, IEEE Trans. on Plasma Science PS-3 (1975), 1
- 14) for example, H. A. Atwater *Introduction to Microwave Theory* (McGraw-Hill, New York, 1962), Chapter 7.
- 15) L. M. Field, Proc. IRE **37** (1949), 34
- 16) E. L. Chu and W. W. Hansen, J. Appl. Phys. **18** (1947), 996